.

Strong electrically tunable $MoTe_2$/graphene van der Waals heterostructures for high-performance electronic and optoelectronic devices

Feng Wang, Lei Yin, Zhenxing Wang, Kai Xu, Fengmei Wang, Tofik Ahmed Shifa, Yun Huang, Yao Wen, Chao Jiang, and Jun He'

Citation: Appl. Phys. Lett. **109**, 193111 (2016); doi: 10.1063/1.4967232
View online: http://dx.doi.org/10.1063/1.4967232
View Table of Contents: http://aip.scitation.org/toc/apl/109/19
Published by the American Institute of Physics

RIGHTSLINK
Copyright Clearance Center

APPLIED PHYSICS LETTERS **109**, 193111 (2016)

Strong electrically tunable $MoTe_2$/graphene van der Waals heterostructures for high-performance electronic and optoelectronic devices

Feng Wang,[1,2] Lei Yin,[1,2] Zhenxing Wang,[1] Kai Xu,[1,2] Fengmei Wang,[1,2]
Tofik Ahmed Shifa,[1,2] Yun Huang,[1,2] Yao Wen,[1,2] Chao Jiang,[1] and Jun He[1,a)]
[1]*CAS Center for Excellence in Nanoscience, CAS Key Laboratory of Nanosystem and Hierarchical Fabrication, National Center for Nanoscience and Technology, Beijing 100190, China*
[2]*University of Chinese Academy of Sciences, Beijing 100049, People's Republic of China*

(Received 23 September 2016; accepted 25 October 2016; published online 8 November 2016)

$MoTe_2$ is an emerging two-dimensional layered material showing ambipolar/p-type conductivity, which makes it an important supplement to n-type two-dimensional layered material like MoS_2. However, the properties based on its van der Waals heterostructures have been rarely studied. Here, taking advantage of the strong Fermi level tunability of monolayer graphene (G) and the feature of van der Waals interfaces that is free from Fermi level pinning effect, we fabricate G/$MoTe_2$/G van der Waals heterostructures and systematically study the electronic and optoelectronic properties. We demonstrate the G/$MoTe_2$/G FETs with low Schottky barriers for both holes (55.09 meV) and electrons (122.37 meV). Moreover, the G/$MoTe_2$/G phototransistors show high photoresponse performances with on/off ratio, responsivity, and detectivity of $\sim 10^5$, 87 A/W, and 10^{12} Jones, respectively. Finally, we find the response time of the phototransistors is effectively tunable and a mechanism therein is proposed to explain our observation. This work provides an alternative choice of contact for high-performance devices based on p-type and ambipolar two-dimensional layered materials. *Published by AIP Publishing*. [http://dx.doi.org/10.1063/1.4967232]

Two-dimensional layered materials (2DLMs), including graphene, transition metal dichalcogenides (TMDs),[1–3] black phosphorene,[4] etc., have received a great deal of scientific interest due to their novel properties and promising potentials in next-generation electronic and optoelectronic devices.[5] In addition, van der Waals heterostructures (vdWHs), obtained by artificially stacking 2DLM layers upon each other, not only greatly enrich the choices of materials with desired properties but also provide a possibility of constructing functional structures, making 2DLMs a more fascinating material family.[6,7] However, one major challenge while fabricating high-performance devices on 2DLMs is the existence of large Schottky barriers (SBs) at the electrode contact interfaces due to the invalidation of the traditional doping method that would seriously destroy the 2DLMs.[8] So far, a number of strategies have been developed to reduce the contact SBs.[9,10] Among them, using graphene (G) as contact may be the most promising choice because of its ultrahigh carrier mobility, excellent mechanical properties, and universality with extensive 2DLMs due to the strong Fermi level tunability.[11] However, the so-far research is mainly limited to G/MoS_2, and p-type or ambipolar 2DLMs have been rarely studied.[7,12,13] More importantly, the photoresponse properties of G/2DLMs structures have been few involved. As a result, more study is urgently needed.

$MoTe_2$ is an emerging 2DLM showing ambipolar/p-type conduction with the hole mobility of 0.2 to 50 $cm^2\ V^{-1}\ s^{-1}$, making it an important supplement to n-type 2DLMs like MoS_2.[3,14] With a bandgap value of $\sim$1.0 eV in the bulk state, $MoTe_2$ and its vdWHs have attracted great attention.[15,16] Recently, our group fabricated $MoTe_2$ FETs and demonstrated ultrahigh photoresponse performances.[16] However, considerable SBHs were also observed. At the time of preparing this manuscript, we notified two works that fabricated and studied $MoTe_2$/G vdWHs.[17] Nevertheless, the "graphene" utilized was 6/24 nm and bilayer in thickness. Considering the strong dependence of the Fermi level tunability of graphene on its thickness,[11] it is essential to study the $MoTe_2$/G vdWHs constructed with "true" monolayer graphene.

Herein, we have fabricated $MoTe_2$/monolayer G vdWHs and systematically studied its electronic and optoelectronic properties. We demonstrate the G/$MoTe_2$/G FETs with low SBHs for both holes (55.09 meV) and electrons (122.37 meV). Moreover, the G/$MoTe_2$/G phototransistor also shows a good photoresponse performance under an illumination of a 473 nm laser with on/off ratio, responsivity, and detectivity of as high as $\sim 10^5$, 87 A/W, and 10^{12} Jones, respectively. To a greater extent, we find that the photoresponse time is effectively tunable, and a mechanism based on the gate voltage dependent depletion region is proposed to explain our observation. We believe that our work provide an alternative choice of contact for p-type and ambipolar 2DLMs with high electronic and optoelectronic performances.

To fabricate our devices, monolayer graphene was used with the thickness defined by the Raman spectrum as typically shown in Fig. 1(c). The obvious G 1586 (cm^{-1}) and 2D (2681 cm^{-1}) peaks with an intensity ratio of $I_G/I_{2D} \approx 0.5$ were detected, confirming the monolayer nature.[18] In addition, the homogeneity of graphene electrodes was further confirmed by Raman mapping (see Figure S6 in the supplementary material). The two-terminal graphene electrode pattern was obtained by

a)Author to whom correspondence should be addressed. Electronic mail: hej@nanoctr.cn

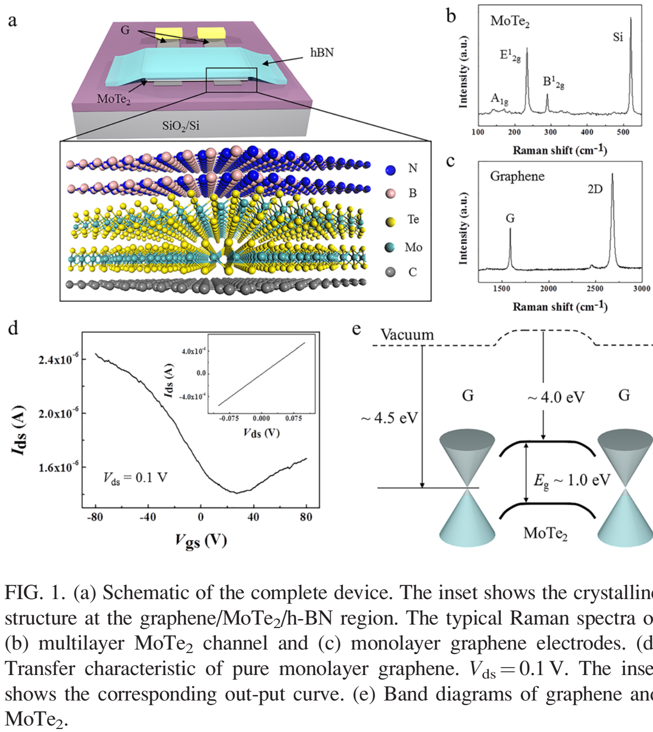

FIG. 1. (a) Schematic of the complete device. The inset shows the crystalline structure at the graphene/$MoTe_2$/h-BN region. The typical Raman spectra of (b) multilayer $MoTe_2$ channel and (c) monolayer graphene electrodes. (d) Transfer characteristic of pure monolayer graphene. $V_{ds} = 0.1$ V. The inset shows the corresponding out-put curve. (e) Band diagrams of graphene and $MoTe_2$.

standard electron beam lithography (EBL) and reactive ion etching (RIE) processes. And 10/60 nm Cr/Au was used as the electrode leads. Figure 1(d) shows the output and transfer characteristics of the pure graphene electrode. The perfect linear drain current-voltage bias (I_{ds}-V_{ds}) curve confirms a good contact quality between Cr/Au and G. In addition, the graphene FET shows a slightly p-type conduction behavior, which agrees with the previous results of graphene on the SiO_2/Si substrate.[11] $MoTe_2$ flakes were then exfoliated and transferred onto the as-fabricated graphene electrodes through wet or dry methods (see the supplementary material for details). The characteristic Raman-active modes of A_{1g} (171 cm^{-1}), $E^1{}_{2g}$ (233 cm^{-1}), and $B^1{}_{2g}$ (289 cm^{-1}) were clearly observed as shown in Figure 1(b), demonstrating the good quality of $MoTe_2$ after the transfer process.[19] Finally, hexagonal boron nitride (hBN) was exfoliated and transferred onto the $MoTe_2$ channels to protect the devices from any possible degradation. Figure 1(a) depicts the schematic drawing of the complete device, with the cross-sectional crystalline structure shown in the enlarged view.

Considering the work function of graphene ($\sim$4.5 eV),[11,12] the electron affinity and the bandgap of $MoTe_2$ ($\sim$4.0 and 1.0 eV for multilayers, respectively),[16,20] the band diagram of the device is depicted in Figure 1(e). Interestingly, the Dirac point of the G electrodes locates nearly at the middle of the bandgap of $MoTe_2$. In view of the strong Fermi level tunability of monolayer graphene,[11] the feature of vdW interface, which is free from the Fermi level pinning effect, and the small bandgap of $MoTe_2$, small SBHs might be induced both for holes and electrons conductions.

Figure 2(a) shows the optical microscope (OM) image of the G/$MoTe_2$/G device obtained by the dry transfer method. The perfect linear output curves under variable gate voltages (V_{gs}) were observed as shown in Figure 2(b), demonstrating the good quality of G/$MoTe_2$ heterostructures. Temperature-dependent transport properties were then carried out to quantitatively study the SBHs of our device (Figure 2(c)). According to the thermionic emission theory, the current injected through a SB to 2DLM is[21]

$$I_{ds} = A^* S T^{3/2} \exp\left[-\frac{1}{k_B T}\left(E_A - \frac{qV_{ds}}{n}\right)\right], \tag{1}$$

where A^* is Richardson constant, S is the contact area, T is the temperature, k_B is the Boltzmann constant, q is the electron charge, n is the ideality factor coming from image charge, and E_A is the total activation energy that charge carriers need to overcome to inject onto the channel and equals to SBH ($q\Phi_B$) when the flat-band condition is met. To determine the SBH, the $\ln(I_{ds}/T^{3/2})$ in dependence of the reciprocal temperature $1000/T$ was plotted for various gate voltages (Figure 2(d)). Two parts with different slopes against temperature were observed, indicating that the thermionic emission/tunneling dominates the current for the high/low temperature range, respectively. Through fitting the linear part at high temperature range, we can obtain $-(E_A\text{-}qV_{ds}/n)/1000k_B$ from the slope (S_p) for variable gate voltages. Figure 2(e) shows the calculated $E_A\text{-}qV_{ds}/n$ as a function of V_{gs} for $V_{ds} = 2$ V as an example. The results for $V_{ds} = 0.5$, 1, and 1.5 V are shown in Figure S1 in the supplementary material. The data exhibit two linear parts and approach flats at $V_{gs} = -37$ and 20 V, where the flat band conditions for holes and electrons injection are realized (i.e., $E_A = q\Phi_B$), respectively.[8] By plotting the S_p values at flat band conditions as a function of V_{ds}, we can then extract $q\Phi_B$ from the y-intercepts through $S_{p0} = q\Phi_B/1000k_B$ (Figure 2(f)).

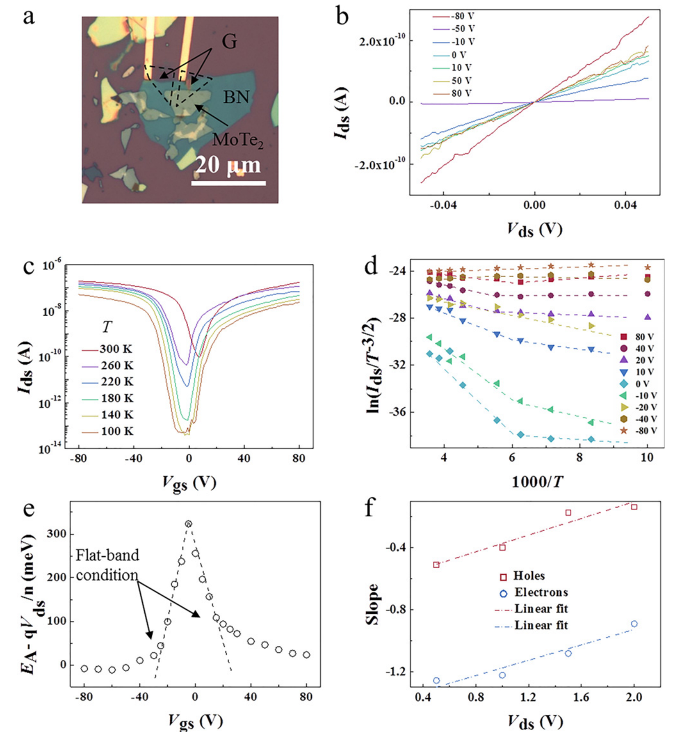

FIG. 2. (a) Optical microscope image of the device. (b) Out-put characteristics under variable gate voltages. (c) Temperature-dependent transfer characteristics, $V_{ds} = 2$ V. (d) The Arrhenius plot of $\ln(I_{ds}/T^{3/2})$ vs. $1000/T$. (e) The extracted $E_A\text{-}qV_{ds}/n$ as a function V_{gs}. The flat conditions are realized at the points where the values stop depending linearly on V_{gs}. (f) The voltage bias dependent slopes at the points where flat conditions are realized. The linear fittings are shown as dashed-dotted lines.

RIGHTSLINK

TABLE I. Summary of the fabrication method, thickness of the $MoTe_2$ channels, and extracted Schottky barrier heights for holes and electrons injection. The null values come from the absence of flat conditions in the measurement range.

Method	Device	Thickness (nm)	SBH for holes (meV)	SBH for electrons (meV)
Dry transfer	With BN #1	8.9	55.09	122.37
	With BN #2	7.6	36.35	
Wet transfer	Without BN #3	9.4	113.97	186.29
	Without BN #4	1.4	69.09	
	With BN #5	6.2	175.15	286.6
	With BN #6	4.5	124.83	

For the device shown in Figure 2(a), the $q\Phi_B$ was calculated to be 55.09 meV for holes, which is comparable with that of MoS_2 FETs with Sc contacts,[9] and 122.37 meV for electrons, respectively.

Five other devices with different $MoTe_2$ thicknesses were also fabricated (see Figures S2–S5 in the supplementary material), and the results are summarized in Table I. We found that the G/$MoTe_2$/G FETs display a symmetric ambipolar to p-dominant conduction behavior transition while reducing the $MoTe_2$ thickness, which is probably due to the thickness-dependent bandgap modulation/surface states proportion.[22] For either conduction behavior, smaller SBHs were observed for the G/$MoTe_2$/G FETs obtained by the dry transfer method, which is possibly because of the higher quality of G/$MoTe_2$ interfaces. Notably, due to the strong Fermi level tunability, the graphene contacts not only enable a small SBH for holes but also a fairly low SBH for electrons in $MoTe_2$ FETs.

We then studied the photoresponse properties of the heterostructure (Figure S6(a) in the supplementary material). To eliminate the influence of the probable photo-thermal effect, the characterization was carried out at low temperature condition (100 K). A 473 nm laser with variable power densities

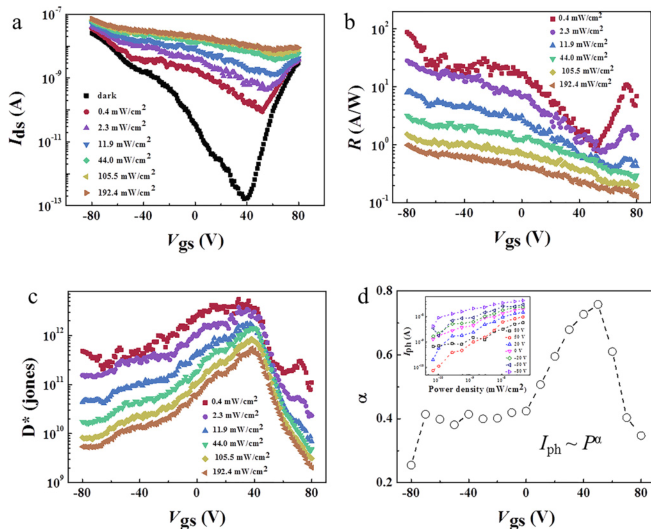

FIG. 3. (a) Transfer characteristics under dark and illumination states. The corresponding (b) responsivity and (c) detectivity as a function of gate voltage under variable illumination densities. The photocurrent change with light power density for variable gate voltages is shown in the inset of (d). (d) The extracted relationship between α and gate voltage.

of 0.424–192.389 mW/cm^2 was used as the light source. Figure 3(a) shows the transfer characteristics under dark and illumination states. A remarkable increase in I_{ds} was detected even for a light power down to $\sim 10^{-10}$ W (the active area of the device is about 44.6 μm^2, Figure S6(a)), indicating the ultrasensitive photoresponse ability. And a peak I_{ds} on/off ratio of about 7×10^4 was achieved at $V_{gs} = 38$ V. Two other figures of merit were calculated to evaluate the photoresponse performances. The first is responsivity (R) that is defined as $R = I_{ph}/AP_{opt}$, where I_{ph} is the photocurrent given by $I_{ph} = I_{illumination} - I_{dark}$, with $I_{illumination}$ and I_{dark} representing the drain currents of illuminated and dark states, respectively.[2] Similar to the I_{ds}-V_{gs} curves shown in Figure 3(a), the R experiences an ambipolar to p-type behavior transition while increasing P_{opt} (Figure 3(b)), and peak values of 87 and 73 A/W were obtained for p- and n-type conductions, respectively. We attribute this transition to the change of photoconduction mechanism from photogating effect to photovoltaic effect while increasing P_{opt}, which has not been found in $MoTe_2$ phototransistors with metal contacts.[23] Then the external quantum efficiency (EQE) was calculated to be 229 and 192 for hole and electron conductions, respectively, using $EQE = Rhc/q\lambda$, where h, c, and λ are the planch constant, the speed of the incident light, and wavelength of the incident light, respectively. Another merit is Detectivity (D^*) given by $D^* = (A\Delta f)^{1/2}/NEP$, where A is the active area in cm^2, Δf is the electrical bandwidth in Hz, and NEP is the noise equivalent power. By assuming that the dark current dominates the shot noise, D^* then can be rewritten as $D^* = I_{ph}/P_{opt}(2qAI_{dark})^{1/2}$.[24,25] Figure 3(c) displays the V_{gs}-dependent D^*. Unlike I_{ds} or R, the D^* exhibits an "inversely ambipolar" behavior, indicating the dominant role of I_{dark}. Notably, a maximum D^* of 5.5×10^{12} Jones was achieved at $V_{gs} = 29$ V, which is comparable to the commercial Si and GaAs photodetectors.[24] In the range of applied V_{gs}, the photocurrent increased monotonously with the increase in P_{opt} following a relationship of $I_{ph} \propto P_{opt}{}^{\alpha}$, as shown in the inset of Figure 3(d). The V_{gs}-dependent α was extracted and displayed in Figure 3(d). Interestingly, α exhibits a similar dome-like tendency, which is ascribed to the V_{gs} dependent depletion region width (W_d) at the $MoTe_2$/G interfaces (see the later analysis).

The time-dependent photoresponse properties were also studied. The good photoswitching stability can be seen from the I_{ds}-t relationship shown in Figure 4(b). Figure 4(a) displays the time-resolved photocurrent decay process under variable V_{gs}. By defining the decay time (t_D) as the time length it takes for the I_{ds} to decrease to $1/e \approx 37\%$ of its peak value, we can extract t_D for variable V_{gs}. Interestingly, the t_D decrease monotonously while scanning V_{gs} from -80 to 30 V, as shown in Figure 4(c). Here, we just show the t_D at $V_{gs} < 30$ V because of the instrument's resolution limit. For a metal/semiconductor/metal (MSM) photodetector, the temporal response property is determined by two components: the fast charge carriers drift process in the depletion region and the slow diffusion process in the quasi-neutral region.[24,26] For our device, a smaller W_d would be realized at the condition of more negative V_{gs} due to the matched Fermi levels of G and $MoTe_2$. Hence, the long quasi-neutral region dominates the device, and larger t_D was induced (the up

RIGHTSLINK Copyright Clearance Center

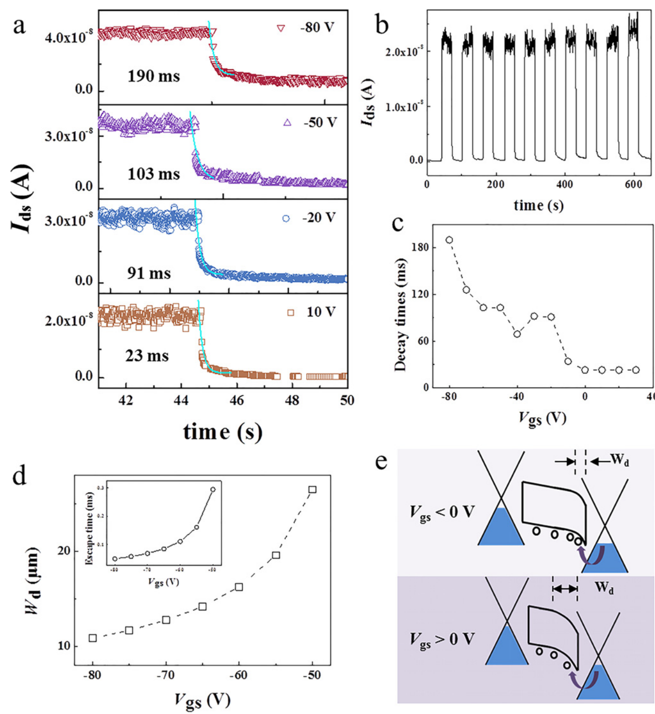

FIG. 4. (a) Time-resolved photocurrent decay process under variable gate voltages. The time axis (x axis) for $V_{gs} = -80$ to -20 V is not shown for the sake of brevity. The green curves are the exponential fits. $V_{ds} = 2$ V. $P_{opt} = 192.4$ mW/cm^2. (b) The long-term stability of the phototransistor. (c) The relationship between decay time and gate voltage. (d) The calculated depletion region widths for variable gate voltages. The inset shows the calculated time lengths for charge carriers to escape the depletion regions. (e) Schematic band profiles while $V_{gs} < 0$ V (top panel) and $V_{gs} > 0$ V (bottom panel).

panel in Figure 4(e)). On the other hand, smaller t_D was induced due to the increased W_d (the bottom panel in Figure 4(e)). For the same reason, the I_{ph}-P_{opt} relationships exhibit a dome-like transition as shown in Figure 3(d). To be specific, the t_D can be tuned to be lower than 23 ms at $V_{gs} > 0$ V.

To verify the above image, a semi-quantitative calculation was carried out. The calculation method is given in the supplementary material. Figure 4(d) shows the calculated W_d for variable V_{gs}. The W_d increase from $\sim$10 to 26 μm while scanning the V_{gs} from -80 to 50 V, confirming our above hypothesis. Note that the actual scale of W_d should be order(s) smaller than the calculated value because of the overestimation of the voltage drop on the depletion region, and the underestimation of the charge densities by ignoring the massive photogenerated charge carriers. Accordingly, the time for charge carriers to be swept out of the depletion region (t_E) can be determined using $t_E = 2W_D/E_m\mu_p$, where μ_p is the field effective mobility of holes and E_m is the maximum electronic field strength in the depletion region. The t_E increases while increasing V_{gs} and their values are in the scale of 0.1 ms (the inset of Figure 4(d)), demonstrating that the device is actually composed with both depletion region and quasi-neutral region, and the slow diffusion process determines the decay time.

In summary, the electronic and optoelectronic properties of $MoTe_2$/G vdWHs have been systematically studied. Using the dry transfer method, we demonstrated the G/$MoTe_2$/G FETs with SBHs of as low as 55.09 meV for holes and 122.37 meV for electrons in ambipolar $MoTe_2$, and 33.35 meV for holes in p-dominated $MoTe_2$. Moreover, the G/$MoTe_2$/G device structure also showed good photoresponse performances to 473 nm laser with on/off ratio, responsivity and detectivity of as high as $\sim$10^5, 87 A/W and 10^{12} Jones, respectively. To a greater extent, we found the response time of the G/$MoTe_2$/G phototransistors is effectively tunable and a mechanism based on the gate voltage dependent depletion region is proposed to explain our observation. Our work consolidates the general role of graphene electrode for low Schottky barrier contact and provides an alternative choice for p-type or ambipolar 2DLM device with high-performance electronic and optoelectronic properties.

See supplementary material for the experimental and calculation methods, as well as the additional electronic characterizations.

This work was supported by the National Natural Science Foundation of China (Nos. 21373065, 61474033, and 61574050), Strategic Priority Research Program of the Chinese Academy of Sciences (Grant No. XDA09040201), 973 Program of the Ministry of Science and Technology of China (No. 2012CB934103), and CAS Key Laboratory of Nanosystem and Hierarchical Fabrication. The authors also gratefully acknowledge the support of Youth Innovation Promotion Association CAS.

[1] B. Radisavljevic, A. Radenovic, J. Brivio, V. Giacometti, and A. Kis, Nat. Nanotechnol. 6, 147 (2011).
[2] Z. Y. Yin, H. Li, H. Li, L. Jiang, Y. M. Shi, Y. H. Sun, G. Lu, Q. Zhang, X. D. Chen, and H. Zhang, ACS Nano 6, 74 (2012).
[3] Y. F. Lin, Y. Xu, S. T. Wang, S. L. Li, M. Yamamoto, A. Aparecido-Ferreira, W. W. Li, H. B. Sun, S. Nakaharai, W. B. Jian, K. Ueno, and K. Tsukagoshi, Adv. Mater. 26, 3263 (2014); S. Cho, S. Kim, J. H. Kim, J. Zhao, J. Seok, D. H. Keum, J. Baik, D. H. Choe, K. J. Chang, K. Suenaga, S. W. Kim, Y. H. Lee, and H. Yang, Science 349, 625 (2015).
[4] L. K. Li, Y. J. Yu, G. J. Ye, Q. Q. Ge, X. D. Ou, H. Wu, D. L. Feng, X. H. Chen, and Y. B. Zhang, Nat. Nanotechnol. 9, 372 (2014).
[5] S. Z. Butler, S. M. Hollen, L. Y. Cao, Y. Cui, J. A. Gupta, H. R. Gutierrez, T. F. Heinz, S. S. Hong, J. X. Huang, A. F. Ismach, E. Johnston-Halperin, M. Kuno, V. V. Plashnitsa, R. D. Robinson, R. S. Ruoff, S. Salahuddin, J. Shan, L. Shi, M. G. Spencer, M. Terrones, W. Windl, and J. E. Goldberger, ACS Nano 7, 2898 (2013); F. Wang, Z. X. Wang, Q. S. Wang, F. M. Wang, L. Yin, K. Xu, Y. Huang, and J. He, Nanotechnology 26, 292001 (2015).
[6] F. Wang, Z. X. Wang, K. Xu, F. M. Wang, Q. S. Wang, Y. Huang, L. Yin, and J. He, Nano Lett. 15, 7558 (2015); A. K. Geim and I. V. Grigorieva, Nature 499, 419 (2013); C. H. Lee, G. H. Lee, A. M. van der Zande, W. C. Chen, Y. L. Li, M. Y. Han, X. Cui, G. Arefe, C. Nuckolls, T. F. Heinz, J. Guo, J. Hone, and P. Kim, Nat. Nanotechnol. 9, 676 (2014).
[7] X. Cui, G. H. Lee, Y. D. Kim, G. Arefe, P. Y. Huang, C. H. Lee, D. A. Chenet, X. Zhang, L. Wang, F. Ye, F. Pizzocchero, B. S. Jessen, K. Watanabe, T. Taniguchi, D. A. Muller, T. Low, P. Kim, and J. Hone, Nat. Nanotechnol. 10, 534 (2015); T. Roy, M. Tosun, J. S. Kang, A. B. Sachid, S. B. Desai, M. Hettick, C. M. C. Hu, and A. Javey, ACS Nano 8, 6259 (2014).
[8] A. Allain, J. H. Kang, K. Banerjee, and A. Kis, Nat. Mater. 14, 1195 (2015).
[9] S. Das, H. Y. Chen, A. V. Penumatcha, and J. Appenzeller, Nano Lett. 13, 100 (2013).
[10] R. Kappera, D. Voiry, S. E. Yalcin, B. Branch, G. Gupta, A. D. Mohite, and M. Chhowalla, Nat. Mater. 13, 1128 (2014).
[11] Y. J. Yu, Y. Zhao, S. Ryu, L. E. Brus, K. S. Kim, and P. Kim, Nano Lett. 9, 3430 (2009).
[12] L. L. Yu, Y. H. Lee, X. Ling, E. J. G. Santos, Y. C. Shin, Y. X. Lin, M. Dubey, E. Kaxiras, J. Kong, H. Wang, and T. Palacios, Nano Lett. 14, 3055 (2014).
[13] Y. Liu, H. Wu, H. C. Cheng, S. Yang, E. B. Zhu, Q. Y. He, M. N. Ding, D. H. Li, J. Guo, N. O. Weiss, Y. Huang, and X. F. Duan, Nano Lett. 15, 3030 (2015); H. J. Chuang, X. B. Tan, N. J. Ghimire, M. M. Perera, B. Chamlagain, M. M. C. Cheng, J. Q. Yan, D. Mandrus, D. Tomanek, and

RIGHTSLINK

Z. X. Zhou, Nano Lett. **14**, 3594 (2014); D. R. Qiu and E. K. Kim, Sci. Rep. **5**, 13473 (2015).
[14]N. R. Pradhan, D. Rhodes, S. M. Feng, Y. Xin, S. Memaran, B. H. Moon, H. Terrones, M. Terrones, and L. Balicas, ACS Nano **8**, 5911 (2014).
[15]K. A. Zhang, T. N. Zhang, G. H. Cheng, T. X. Li, S. X. Wang, W. Wei, X. H. Zhou, W. W. Yu, Y. Sun, P. Wang, D. Zhang, C. G. Zeng, X. J. Wang, W. D. Hu, H. J. Fan, G. Z. Shen, X. Chen, X. F. Duan, K. Chang, and N. Dai, ACS Nano **10**, 3852 (2016); A. Pezeshki, S. Hossein, H. Shokouh, T. Nazari, K. Oh, and S. Im, Adv. Mater. **28**, 3216 (2016); F. Wang, L. Yin, Z. X. Wang, K. Xu, F. M. Wang, T. A. Shifa, Y. Huang, C. Jiang, and J. He, Adv. Funct. Mater. **26**, 5499 (2016).
[16]L. Yin, X. Y. Zhan, K. Xu, F. Wang, Z. X. Wang, Y. Huang, Q. S. Wang, C. Jiang, and J. He, Appl. Phys. Lett. **108**, 043503 (2016).
[17]K. Choi, Y. T. Lee, J. S. Kim, S. W. Min, Y. Cho, A. Pezeshki, D. K. Hwang, and S. Im, Adv. Funct. Mater. **26**, 3146 (2016); M. Kuiri, B. Chakraborty, A. Paul, S. Das, A. K. Sood, and A. Das, Appl. Phys. Lett. **108**, 063506 (2016).
[18]A. C. Ferrari, J. C. Meyer, V. Scardaci, C. Casiraghi, M. Lazzeri, F. Mauri, S. Piscanec, D. Jiang, K. S. Novoselov, S. Roth, and A. K. Geim, Phys. Rev. Lett. **97**, 187401 (2006).
[19]C. Ruppert, O. B. Aslan, and T. F. Heinz, Nano Lett. **14**, 6231 (2014).
[20]T. Boker, R. Severin, A. Muller, C. Janowitz, R. Manzke, D. Voss, P. Kruger, A. Mazur, and J. Pollmann, Phys. Rev. B **64**, 235305 (2001).
[21]S. Sze and K. N. Kwok, *Physics of Semiconductor Devices* (Wiley Online Library, Hoboken, NJ, USA, 2007).
[22]D. J. Perello, S. H. Chae, S. Song, and Y. H. Lee, Nat. Commun. **6**, 7809 (2015); J. J. Fonseca, S. Tongay, M. Topsakal, A. R. Chew, A. J. Lin, C. Ko, A. V. Luce, A. Salleo, J. Wu, and O. D. Dubon, Adv. Mater. **28**, 6465 (2016).
[23]Q. S. Guo, A. Pospischil, M. Bhuiyan, H. Jiang, H. Tian, D. Farmer, B. C. Deng, C. Li, S. J. Han, H. Wang, Q. F. Xia, T. P. Ma, T. Mueller, and F. N. Xia, Nano Lett. **16**, 4648 (2016).
[24]W. Zhang, M. H. Chiu, C. H. Chen, W. Chen, L. J. Li, and A. T. S. Wee, ACS Nano **8**, 8653 (2014).
[25]K. K. Manga, S. Wang, M. Jaiswal, Q. L. Bao, and K. P. Loh, Adv. Mater. **22**, 5265 (2010).
[26]J. P. Clifford, G. Konstantatos, K. W. Johnston, S. Hoogland, L. Levina, and E. H. Sargent, Nat. Nanotechnol. **4**, 40 (2009); K. Xu, Z. X. Wang, F. Wang, Y. Huang, F. M. Wang, L. Yin, C. Jiang, and J. He, Adv. Mater. **27**, 7881 (2015).

RIGHTSLINK